Arctic Tropospheric Winds Derived from TOVS Satellite Retrievals

JENNIFER A. FRANCIS AND ELIAS HUNTER

Institute of Marine and Coastal Sciences, Rutgers–The State University of New Jersey, New Brunswick, New Jersey

CHENG-ZHI ZOU

Office of Research and Applications, NOAA/NESDIS, Camp Springs, Maryland

(Manuscript received 17 December 2003, in final form 16 November 2004)

ABSTRACT

Accurate three-dimensional wind fields are essential for diagnosing a variety of important climate processes in the Arctic, such as the advection and deposition of heat and moisture, changes in circulation features, and transport of trace constituents. In light of recent studies revealing significant biases in upper-level winds over the Arctic Ocean from reanalyses, new daily wind fields are generated from 22.5 yr of satellite-retrieved thermal-wind profiles, corrected with a recently developed mass-conservation scheme. Compared to wind measurements from rawinsondes during the Surface Heat Budget of the Arctic (SHEBA) experiment, biases in satellite-retrieved winds are near zero in the meridional direction, versus biases of over 50% for reanalyses. Errors in the zonal component are smaller than those observed in reanalysis winds in the upper troposphere, while in the lower troposphere the effects of Greenland introduce uncertainty in the mass-conservation calculation. Further reduction in error may be achieved by incorporating winds retrieved from feature-tracking techniques using satellite imagers. Overall, satellite-retrieved winds are superior to reanalysis products over the data-sparse Arctic Ocean and provide increased accuracy for analyses requiring wind information.

Trends and anomalies for the 22.5-yr record are calculated for both meridional and zonal winds at eight levels between the surface and 300 hPa. Annual mean trends are similar at varying levels, reflecting the relatively barotropic nature of the Arctic troposphere. Zonal winds are more westerly over Eurasia and the western Arctic Ocean, while westerlies have weakened over northern Canada. Combined with the corresponding pattern in meridional winds, these results suggest that the polar vortex has, on average, shifted toward northern Canada. Seasonal trends show that some changes persist throughout the year while others vary in magnitude and sign. Most striking are spring patterns, which differ markedly from the other seasons. Changes in meridional winds are consistent with observed trends in melt-onset date and sea ice concentration in the marginal seas. Anomalies in zonal wind profiles exhibit decadal-scale cyclicity in the eastern Arctic Ocean, while overall shifts in anomaly signs are evident and vary by region. The winter North Atlantic Oscillation (NAO) index correlates moderately with meridional wind anomalies in the Atlantic sector of the Arctic Ocean: positively (0.48) in the Barents Sea and negatively (-0.59) in the Lincoln Sea. These observed trends and anomalies are expected to translate to changes in advected heat and moisture into the Arctic basin, which are likely linked to trends in sea ice extent, melt onset, cloud properties, and surface temperature.

1. Introduction

Numerous recent studies reveal a plethora of evidence that the Arctic environment has undergone rapid, perhaps unprecedented, change in the past few decades (e.g., Overland et al. 2003; Serreze et al. 2000; Overpeck et al. 1997). Among these is a significant decrease in sea level pressure (Walsh et al. 1996), a fundamental atmospheric parameter that governs surface wind patterns, sea ice motion, and air–surface turbulent energy exchange. To understand the observed changes, as well as their roles in a variety of climate applications—such as analyses of circulation features and disposition of advected energy, moisture, and trace constituents—accurate upper-level wind fields are re-

Corresponding author address: Jennifer Francis, Institute of Marine and Coastal Sciences, Rutgers–The State University of New Jersey, 74 Magruder Rd., Highlands, NJ 07732.
E-mail: francis@imcs.rutgers.edu

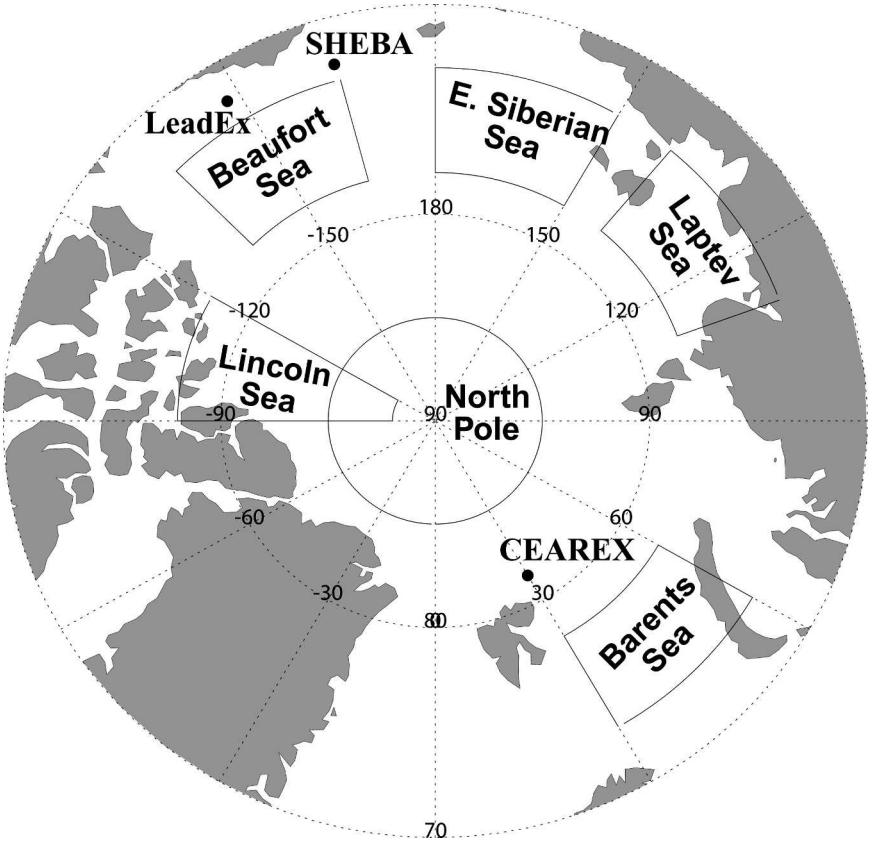

FIG. 1. Approximate locations of the CEAREX, LeadEx, and SHEBA field experiments, and regions defined for time series and anomaly analysis.

quired. Over regions of the world where conventional data are sufficiently dense, the operational reanalyses fulfill this requirement with products that are generally faithful to reality. In high latitudes, however, where observations are sparse (fewer than five observations per 2.5° latitude–longitude box month^{-1}; Kistler et al. 2001), the accuracy of reanalysis products in upper levels is uncertain. This is especially true over the Arctic and Southern Oceans, where rawinsonde data are typically limited to coastal stations, passing ships, temporary ice stations, and short-duration field programs.

Validation of products from reanalyses is notoriously difficult, as their data assimilation procedures ingest as many observations as possible. Independent data, consequently, are few. By comparing the time and location of assimilated rawinsonde data with the sites of rawinsondes from field campaigns in the Arctic region, Francis (2002) ascertained that observations from two field programs were not ingested by the National Centers for Environmental Prediction–National Center for Atmospheric Research (NCEP–NCAR) nor the European Centre for Medium-Range Weather Forecasts (ECMWF) reanalyses, and therefore constitute independent data. The Coordinated Eastern Arctic Experiment [(CEAREX) Drift Group 1990] was conducted northeast of Spitsbergen in the fall/winter of 1988, and the Lead Experiment [(LeadEx) Group 1993] took place in the Beaufort Sea in the spring of 1992 (Fig. 1; Table 1). A comparison of reanalysis upper-level winds with rawinsondes from CEAREX and LeadEx revealed significant differences (Francis 2002). At all levels between the surface and 300 hPa, the biases in u and v wind components from both reanalyses were comparable in magnitude to the observed mean u and v wind speeds. Reanalysis winds were too westerly and northerly, with mean values approximately double those from rawinsondes. The errors in u-component winds appeared to be primarily from differences in speed rather than sign, while negative v biases appeared to result mainly from sign differences. It should be noted that the CEAREX and LeadEx sites were located relatively near to coastal stations (100–300 km), thus differences between reanalysis and measured winds may be larger farther from the coasts. Observations from the Bear Island weather station (74.5°N, 19.0°E), whose rawinsonde data *are* assimilated by the reanalyses, were

TABLE 1. Regions defined for time series and anomaly analysis. Also see Fig. 1 for region locations.

Region name	Lat bounds	Lon bounds
Barents Sea	73°–78°N	30°–60°E
Laptev Sea	73°–78°N	110°–140°E
East Siberian Sea	73°–78°N	150°E–180°
Beaufort Sea	73°–78°N	195°–225°E
Lincoln Sea	78°–88°N	240°–270°E
North Pole	85°–90°N	0°–360°

also compared to reanalysis winds. Biases were only 2% of observed values, and root-mean-square errors were about 60% smaller than those from the unassimilated data locations. For further details, see Francis (2002).

These errors have serious implications for using reanalysis wind fields for Arctic climate research. Overly strong westerlies suggest that the meridional temperature gradients near the experiment sites are too strong, possibly leading to an overly intense, narrow jet stream and/or misplaced cyclonic disturbances. Alternatively the jet axis may be rotated clockwise from its actual alignment, which for a constant speed, could cause the u component to be too positive while the v component is too negative. Winds that are too frequently from the north may imply that semipermanent features in the upper-level circulation may be misplaced and that reanalyses may not properly capture the synoptic-scale features that tend to cause fluctuations, especially in the meridional wind component. Further, if one used reanalysis winds to advect energy or moisture, for example, values would likely be too small in the poleward sense, as the meridional wind is too strong from the north, and transport would be too large in the zonal direction owing to the wind being too strong from the west on average. Models using these winds to calculate surface fluxes or to force sea ice motion may produce patterns with unrealistic features, although errors near the surface are smaller in absolute magnitude.

It is clear from these findings, as well as those by Wang et al. (2003), that more accurate upper-level wind fields over the Arctic Ocean are needed. A possible method to obtain three-dimensional winds is to retrieve them from satellite-derived temperature profiles using the thermal-wind relationship. This was attempted by Peterson and Horn (1977) and Moyer et al. (1978) using data from the *Nimbus-6* satellite and near-surface geostrophic winds estimated from pressure fields over the ocean. These results were generally within 5 m s^{-1} of rawinsonde measurements (Carle and Scoggins 1981). Slonaker and Van Woert (1999) also calculated upper-level, meridional winds from a combination of satellite-derived surface winds and temperature profiles over the Southern Ocean. They then applied these wind fields to the calculation of poleward moisture fluxes. A thermal-wind-only technique, however, does not account for ageostrophic flows, and consequently does not conserve mass. The nonmass-conserved wind has an unrealistic mean meridional circulation structure (Zou and Van Woert 2001, hereafter ZVW1). When ZVW1 augmented this retrieval with a mass-conservation algorithm, the meridional circulation structure was improved, and the retrieved meridional moisture fluxes were reduced by a factor of 2. Subsequently Zou and Van Woert (2002; hereafter ZVW2) generated a dataset of zonal and meridional winds over the Southern Ocean from temperature profiles retrieved from the Television Infrared Observation Satellite (TIROS) Operational Vertical Sounder (TOVS) using their mass-conserving, thermal-wind-based algorithm.

In this paper we adapt the techniques developed for the Southern Ocean by Slonaker and Van Woert (1999) and ZVW2 to the Arctic. We retrieve a new, three-dimensional Arctic wind product from satellite-derived temperature profiles combined with surface pressure fields and 10-m winds from the NCEP–NCAR reanalysis. The correction scheme developed by ZVW2 is applied to ensure mass conservation in both the meridional and zonal directions. We compare these fields with rawinsonde observations from the year long Surface Heat Budget of the Arctic (SHEBA) field project (Uttal et al. 2002), which was conducted in the Beaufort Sea beginning in October 1997 (Fig. 1). Finally we present an analysis of trends and anomalies in zonal and meridional wind components at two representative levels over the 22.5-yr record. These patterns may aid in explaining observed changes in sea ice extent in regions where wind forcing is dominant, and they likely contribute to changes in advective heating, net precipitation, and cloud formation.

2. Methodology

The wind retrieval algorithm begins by obtaining temperature profiles retrieved from the TOVS instrument using the Improved Initialization Inversion (3I) algorithm (Chédin et al. 1985; Scott et al. 1999), which includes modifications to improve accuracy over snow- and sea ice–covered areas (Francis 1994). Twenty years of gridded TOVS products were generated as the so-called Path-P dataset (Francis and Schweiger 2000; Schweiger et al. 2002; Francis and Schweiger 1999) and distributed by the National Snow and Ice Data Center (NSIDC). In this study we use ungridded orbital retrievals (Level-2) produced as a part of the Path-P proj-

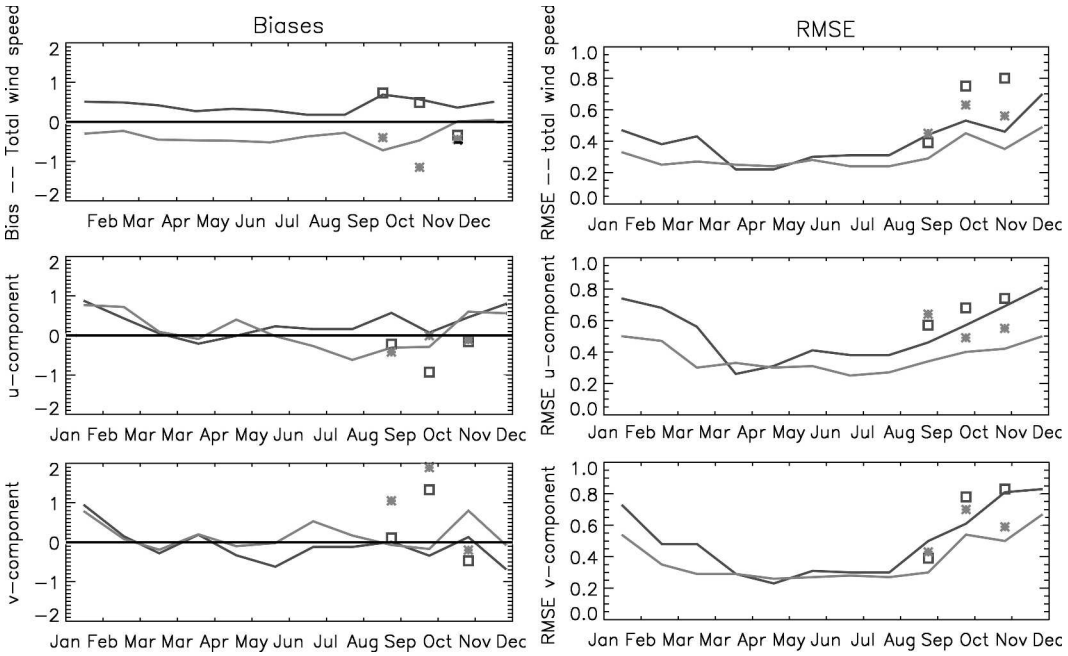

FIG. 2. Summary statistics comparing NCEP–NCAR (red) and ECMWF (blue) reanalysis 10-m winds to measured winds at Russian "North Pole" meteorological stations in 1988. Symbols are comparisons to CEAREX measurements. (left) The biases, (right) the rmses, (top) total wind speed, (middle) u (zonal) wind component, and (bottom) v (meridional) wind component.

ect, and recently extended through 2001. The TOVS instruments used for this study flew on the National Oceanic and Atmospheric Administration (*NOAA*) polar-orbiting platforms *-6*, *-7*, *-9*, *-10*, *-11*, *-12*, and *-14*. The horizontal resolution of the Level-2 retrievals is approximately 100×100 km^2, and areas north of 60°N are viewed about 14 times day^{-1} per satellite. Products are not generated over land with elevation greater than 1000 m. Retrieved temperatures at nine standard levels (1000, 900, 850, 700, 600, 500, 400, 300, and 100 hPa) and the surface within 12 h of 1200 UTC each day are averaged to form daily means, then interpolated to a $1° \times 1°$ grid over the region north of 60°N. Gridded values are filtered zonally and meridionally to remove high-frequency noise. Layer-mean temperatures are then calculated between the standard levels listed above. The daily-mean 10-m winds and surface pressures produced by the NCEP–NCAR reanalysis are obtained from NCAR via ftp and interpolated to this grid. Surface pressures are used to define the layer between the surface and 1000 hPa.

The standard method used to estimate upper-level winds from thermal winds builds upward from the surface. The NCEP–NCAR reanalysis 10-m winds, produced on a Gaussian grid, are used as the starting point, thus it is important to ascertain their accuracy. Ten-meter winds from both NCEP–NCAR and ECMWF reanalyses were compared to measurements from Russian "North Pole" (NP) drifting ice stations during 1988. These data are included in the Comprehensive Ocean–Atmosphere Data Set (COADS; Serreze 1997), which were obtained from the NSIDC. The NCEP–NCAR value nearest to the location of an NP ice station was compared to daily-averaged measurements. Figure 2 presents the resulting monthly biases and root-mean-square errors (rmse) from both the NCEP–NCAR and ECMWF reanalyses. Biases in the NCEP–NCAR reanalysis 10-m total wind speeds are consistently about -0.5 m s^{-1} throughout the year, while for the u and v components the sign fluctuates. Rmses are near 0.3 m s^{-1} in summer and about double that in winter months. ECMWF biases are similar in magnitude but opposite in sign with consistently positive values. Rmses are slightly larger than for NCEP–NCAR winds in winter. Having completed this analysis, we later learned that the NP station winds are assimilated by both reanalyses. Consequently, we assume that these results are "best-case scenario," and that far from NP stations errors may be larger. A comparison to CEAREX measurements (symbols in Fig. 2), which were *not* assimilated, reveals some larger errors but not consistently so, perhaps because the CEAREX site was located near coastal stations. We know of no other independent source of measurements, so the degree of

this uncertainty could not be definitively quantified. Nevertheless, we do not expect errors to increase greatly away from NP stations, as sea level pressure measurements from drifting buoys deployed as a part of the International Arctic Buoy Program/Polar Exchange at the Sea Surface (IABP/POLES) project (Rigor et al. 2000) are also assimilated by the reanalyses and provide reasonable coverage for geostrophic wind calculations.

Thermal winds V_T are computed using the standard method (e.g., Wallace and Hobbs 1977) from the thickness gradients ∇Z_T in each layer and in the zonal and poleward directions:

$$\mathbf{V}_T = \frac{g}{f}\nabla Z_T, \tag{1}$$

where

$$Z_T = \frac{R\overline{T}_V}{g}\ln\frac{p_2}{p_1}. \tag{2}$$

Here R is the dry gas constant, $\overline{T}_V$ is the mean-layer virtual temperature, g is gravity, f is the Coriolis parameter, and p is the pressure at the upper and lower boundaries of each layer. Because the polar atmosphere contains very little water vapor, we use actual temperature in place of virtual temperature with a negligible effect. Thermal winds are added sequentially upward beginning with the NCEP–NCAR 10-m u and v winds to create a first-guess wind profile. Over Greenland where TOVS profiles are not retrieved, we substitute NCEP–NCAR reanalysis winds for levels above 700 hPa. The accuracy of reanalysis winds over Greenland is not known.

Slonaker and Van Woert (1999) calculated upper-level winds from TOVS-retrieved thermal winds in the Southern Ocean with moderate success. Because these fields do not conserve mass, however, they are not suitable for climate studies (ZVW1). ZVW2 later found that results improved markedly in both the general circulation structure and wind speed when a mass-conservation constraint is applied both zonally and meridionally. ZVW2 developed and tested two techniques, both of which integrate the mass-conservation equation (3) in a vertical column of the atmosphere:

$$\nabla \cdot \int_{p_T}^{p_s} \mathbf{V}\, dp = -\omega = -\frac{\partial p}{\partial t}, \tag{3}$$

where p_s is the surface pressure, p_T is the pressure at the top of the column (assumed to be 100 hPa), and $\mathbf{V}$ is the horizontal wind vector. The vertical velocity is represented by ω and $\partial p/\partial t$, where $\omega = 0$ at the top of the column and $\omega = \partial p_s/\partial t$ at the surface. ZVW2 then integrate (3) around a latitude circle and along meridians to get a meridional mass-flux-conservation equation that contains only the meridional wind component.

Their wind retrieval approach includes two steps. The first step is to obtain a first-guess wind profile at selected tropospheric levels by adding the thermal wind derived from TOVS temperature profiles to the corresponding surface wind. The surface winds over the Southern Ocean are derived from satellite passive microwave data measured by the Special Sensor Microwave Imager (SSM/I) using a variational analysis by Atlas et al. (1996). The thermal winds are calculated from TOVS layer-mean temperatures retrieved using the method of Susskind et al. (1997), the so-called Path-A algorithm. The second step is to force the first-guess winds to conserve mass in a variational procedure so the winds satisfy complete dynamic constraints. Specifically, the final wind is obtained by solving a variational function in which the differences between the final wind and the first-guess wind are minimized in a least squares sense subject to the mass-conservation constraint. The two techniques developed by ZVW2 are distinguished by whether the mass-conservation technique is applied separately or simultaneously to the zonal and meridional components. In the separate method the meridional mass-flux-conservation equation is first applied across latitudinal walls to force the first-guess v-component wind to conserve mass. The vertically integrated mass-conservation equation is then used to infer the zonal wind. In the second method, the vertically integrated mass-conservation equation is used to constrain the first-guess u and v winds simultaneously. ZVW2 found that the separate method was substantially more successful in reducing differences between retrieved wind fields and measurements from rawinsondes launched at Macquarie Island in the Southern Ocean. This correction significantly decreased the bias in u from near 4 m s^{-1} to approximately 1 m s^{-1}, and the v bias from about 1.5 to -0.3 m s^{-1}. For further detail on these methods and results see ZVW1 and ZVW2.

In an attempt to extend this work and produce three-dimensional wind fields for the Arctic region with smaller biases and rmses than those calculated in the reanalysis products, we adapt the two mass-conservation methods of ZVW2 to TOVS-derived thermal-wind profiles north of 60°N. Applying their methods to the Arctic is somewhat problematic, however, owing to the existence of Greenland in many of the latitude zones. This is of particular concern in the integration for the u-wind component, as Greenland acts like a barrier below about 700 hPa and frequently generates orographically forced flows, such as katabatic winds, of its own. Having tested several methods to resolve this issue, we

obtained the smallest errors by linearly interpolating retrieved winds on either side of Greenland at each level below 700 hPa. Above 700 hPa we use NCEP–NCAR reanalysis winds, as we do not retrieve temperature profiles from TOVS over high elevation areas, and the flow above 700 hPa should be less affected by the orography. This issue may be revisited in the future using satellite-tracked atmospheric features to obtain upper-level winds over Greenland.

3. Results

a. Validation

Wind fields calculated from the combination of TOVS-retrieved temperature profiles and NCEP–NCAR reanalysis 10-m winds are validated with nearly 1 yr of rawinsonde measurements at the SHEBA site in the Beaufort Sea (Fig. 1). The daily-mean TOVS winds are averaged within 100 km of the SHEBA location, then compared with daily averages of rawinsonde observations. Figure 3 presents summary statistics for both first-guess thermal-wind profiles (no mass conservation) and winds corrected using the ZVW2 mass-conservation scheme in which the meridional and zonal constraint is applied separately. We also apply their simultaneous correction scheme, but consistent with ZVW2's findings, the reduction in error is smaller. Only winds calculated using the separate method are presented.

The results for thermal-wind-only wind retrievals (dashed lines in Fig. 3) show that, like the reanalyses, the biases in the u-component thermal-wind profiles are positive, indicating that retrieved winds are too strong from the west. Unlike the reanalyses, however, the biases do not increase appreciably with height. The retrieval biases are about 1 m s^{-1} at the surface and are approximately constant at 3 m s^{-1} with height above 800 hPa. The biases in v-component thermal-wind profiles also exhibit the same sign as the reanalyses but are about half the magnitude above 700 hPa. The Spearman's rank correlation coefficients are approximately 0.7 for both components (not shown), with rmses increasing with height from 2 to about 10 m s^{-1} near the tropopause. The observed jump in rmse from the surface to the next level above is caused by boundary layer effects and the relatively coarse vertical resolution of TOVS temperature retrievals. Particularly in the winter Arctic, strong near-surface temperature inversions and corresponding vertical wind shears are common, which are difficult to capture precisely with satellite sounders. Note that rmses in rawinsonde winds are estimated to be approximately 2–3 m s^{-1} below the jet stream level (more information available online at http://www.eumetsat.de/en/dps/mpef/products/windsuse.html); thus a significant fraction of the rmse shown in Figs. 3 and 4 may be contributed by errors in rawinsonde measurements.

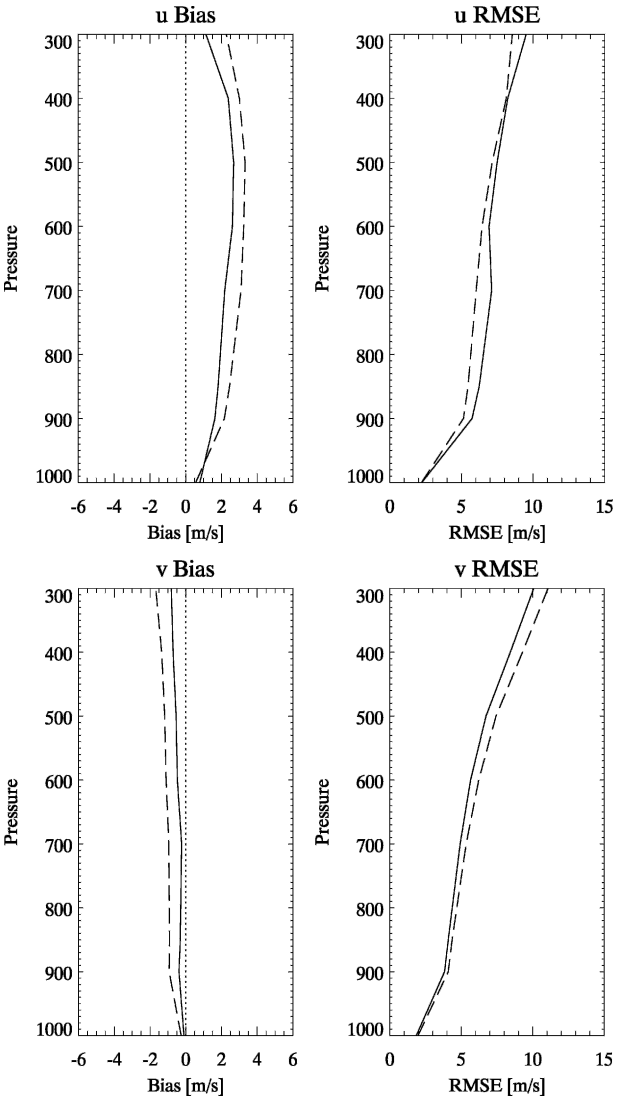

FIG. 3. Error statistics for comparisons of satellite-derived wind profiles with rawinsonde measurements during SHEBA. (top) Zonal (u) winds, (bottom) meridional (v) winds, (left) mean errors (TOVS–SHEBA), and (right) rmses. Dashed lines are thermal-wind profiles with no mass-conservation correction, and solid lines are retrievals with the ZVW2 "separate" mass-conservation method applied.

The solid lines in Fig. 3 are wind retrievals with the ZVW2 mass-conservation correction applied. In all but the rmse for the zonal wind component, errors compared to rawinsondes have clearly been reduced subsequent to applying the mass-conservation constraints. The error reduction for winds in the Arctic is not as substantial, however, as those achieved by ZVW2 in the

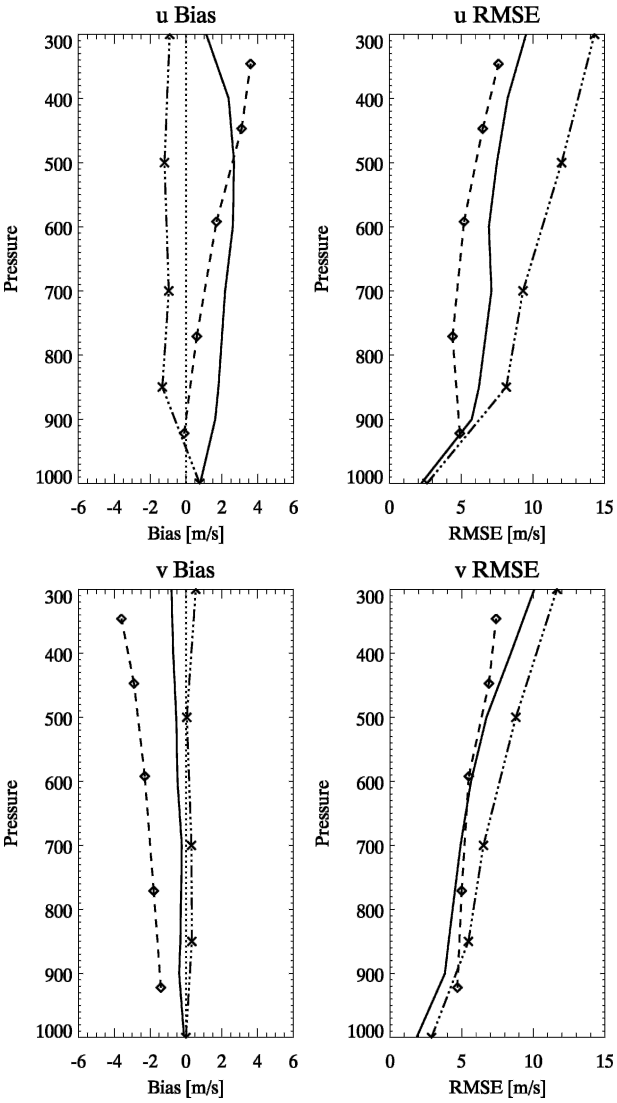

FIG. 4. Comparison of error statistics for polar tropospheric winds from three sources. The dashed line is NCEP–NCAR reanalysis vs rawinsonde data from two Arctic field programs (from Francis 2002); dash–dot line is for TOVS-derived winds vs rawinsonde data from Macquarie Island in the Southern Ocean (from ZVW2); and solid line is for TOVS-derived winds vs SHEBA rawinsondes (from this study).

Southern Ocean. We attribute this to the complicating effects of Greenland in the zonal flow as well as smaller errors in the Arctic first-guess thermal-wind profiles. Biases in the TOVS-derived u winds have decreased 18% on average between the surface and 300 hPa, and biases in v are 66% lower on average owing to the mass-conservation constraint. Average rmses in u are slightly higher (8%) and in v are slightly lower (8%). The dramatic decrease in meridional errors is encouraging for applications of wind retrievals to calculations of poleward moisture and heat advection. We also find a significant improvement in total wind speeds retrieved from TOVS compared with rawinsonde measurements. While NCEP–NCAR and ECMWF reanalyses exhibited biases whose magnitudes were over half of the actual wind speeds, the TOVS-derived biases are only about 10% of total wind speeds.

Figure 4 presents a comparison of biases and rmses for three sources of polar wind information: NCEP–NCAR reanalysis versus rawinsonde measurements from two Arctic field programs (from Francis 2002); TOVS retrievals versus rawinsonde data at Macquarie Island in the Southern Ocean (from ZVW2); and results from this study versus rawinsonde data measured during SHEBA in the Beaufort Sea. Both Arctic wind products (NCEP–NCAR and this study) exhibit positive biases in the zonal component, indicating that winds are stronger from the west than rawinsonde observations. Below 500 hPa the biases in TOVS retrievals are larger than for the NCEP–NCAR reanalysis product, and above this level the NCEP–NCAR errors are larger. We attribute this result to the effects of Greenland in the mass-conservation correction scheme, and also to the fact that the validation site for the reanalysis product is not far from coastal rawinsonde stations, whose data were ingested into the reanalysis. This is also the likely explanation for the reanalysis rmses being smaller than either of the TOVS retrievals. The ZVW2 biases are impressively small, especially considering that the mean zonal winds near Macquarie Island are approximately 5 times stronger than at either of the Arctic sites. While their rmses are larger than the other two sources, it is largely because of the stronger winds. In the meridional direction the two TOVS-derived wind products have very small biases, with values slightly negative in the Arctic and near zero in the Southern Ocean. The biases in the reanalysis product are relatively large and negative, indicating winds in this region are too strong from the north.

In an attempt to account for the effect of mean wind speed on the error statistics, in Fig. 5 we present the same plot as in Fig. 4, but the biases and rmses have been normalized by the mean absolute u and v wind speeds measured by the respective rawinsondes. In the zonal component, the relative bias of the ZVW2 wind is even more impressive, with a value of about 10% of the observed wind speed. The Arctic sources exhibit relative errors that have similarly shaped profiles to those shown in Fig. 4, as mean zonal wind speeds are comparable in the two Arctic regions and time periods. The normalized rmses in the Southern Ocean also outperform the Arctic products. In the meridional component, the two TOVS results exhibit very small percentage biases (less than 10% at all levels) and the relative

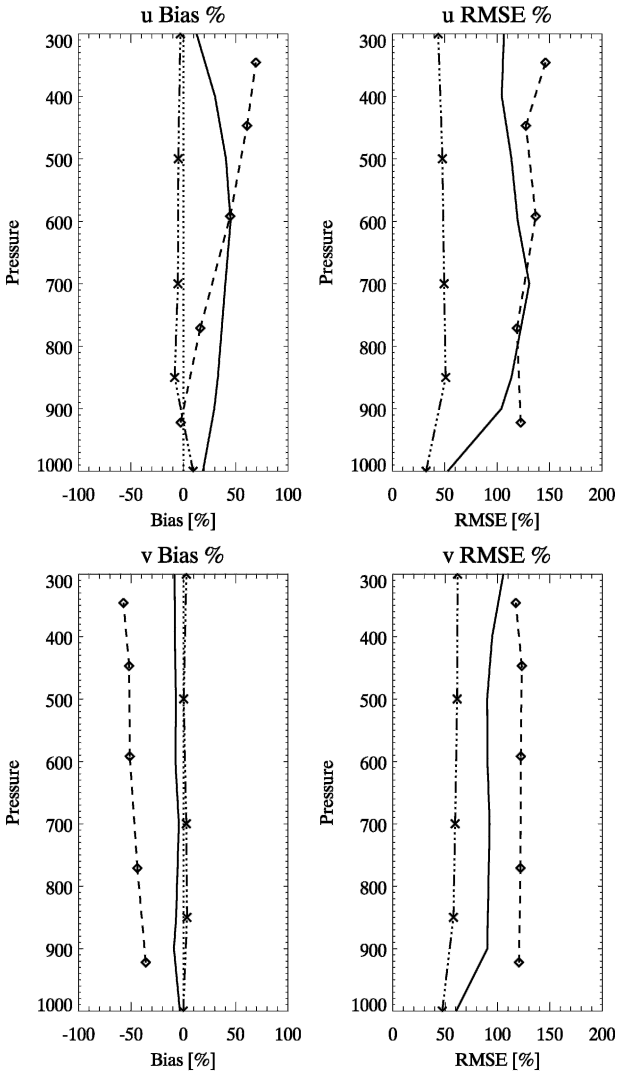

FIG. 5. Same as in Fig. 4, but statistics are normalized by the mean absolute u and v wind magnitudes measured by rawinsondes.

rmses are also smaller than the reanalysis product. These results further support the use of TOVS-derived wind fields, especially the meridional component, for calculations of energy and moisture transport.

b. Trends

Twenty-two and a half years (mid-1979–2001) of TOVS-derived upper-level winds have been used to analyze temporal changes over the Arctic basin. At each latitude–longitude grid point we calculate the least squares linear fit to the u and v wind components, the slope of which is plotted if its significance exceeds the 90% confidence level. Significance is determined as a threshold on the probability density function of the F distribution. Trends are calculated at 1° latitude × longitude resolution for the total troposphere below 300 hPa and for each of the eight levels between the surface and 300 hPa over the entire year and for each season. Note that because thermal winds are derived from horizontal temperature *gradients*, any errors resulting from intra- or intersatellite biases will subtract out, thus analyses of trends and variability are unaffected. Some examples of trend patterns are presented here.

The general wind climatology derived from TOVS-retrieved winds is described for six representative regions of the Arctic (Fig. 1; Table 1). In most areas, the zonal winds at 300 hPa are predominantly positive, as would be expected near the jet stream level. Negative (easterly) excursions occur every few years in the Lincoln and Laptev Seas, however, caused by splitting of the polar vortex with a lobe centered south of the regions. Meridional winds are more variable among the six areas. Barents Sea winds are predominantly from the north, as the area is usually located in the ridge downstream from the Icelandic low. Similarly the Laptev Sea region generally experiences flow from the south owing to the tendency for a trough just west of the area. At 700 hPa, winds are generally weaker, while predominant tendencies in direction are similar.

Figure 6 presents annual trends (meters per second per decade) for the zonal and meridional wind components for the total troposphere, as well as for two representative levels: 300 and 700 hPa. We have compared TOVS-derived trends to those computed from NCEP–NCAR reanalysis winds over land areas where rawinsonde data are relatively dense, and the patterns agree well (not shown). Large areas of significant changes in both u and v are evident in Fig. 6. Our discussion will focus primarily on Arctic Ocean areas where TOVS provides new information.

Zonal winds in much of the eastern Arctic Ocean have become less westerly (from the west) at all levels, while trends in the western Arctic are less cohesive and generally positive. These features, together with positive trends over the northern Eurasian continent, suggest that the polar vortex has strengthened and/or shifted toward the Canadian Archipelago. The pattern in meridional winds is consistent with this explanation, as trends are generally positive near the date line and negative over the Barents–Kara Seas. A tendency toward positive meridional trends over the eastern half of Eurasia suggests increased warm advection, which is consistent with observed changes in surface temperature (e.g., Rigor et al. 2000). Patterns are similar for the total troposphere, 300- and 700-hPa levels, indicating that the atmosphere is, on average, relatively barotropic. The magnitude of total column trends is similar to

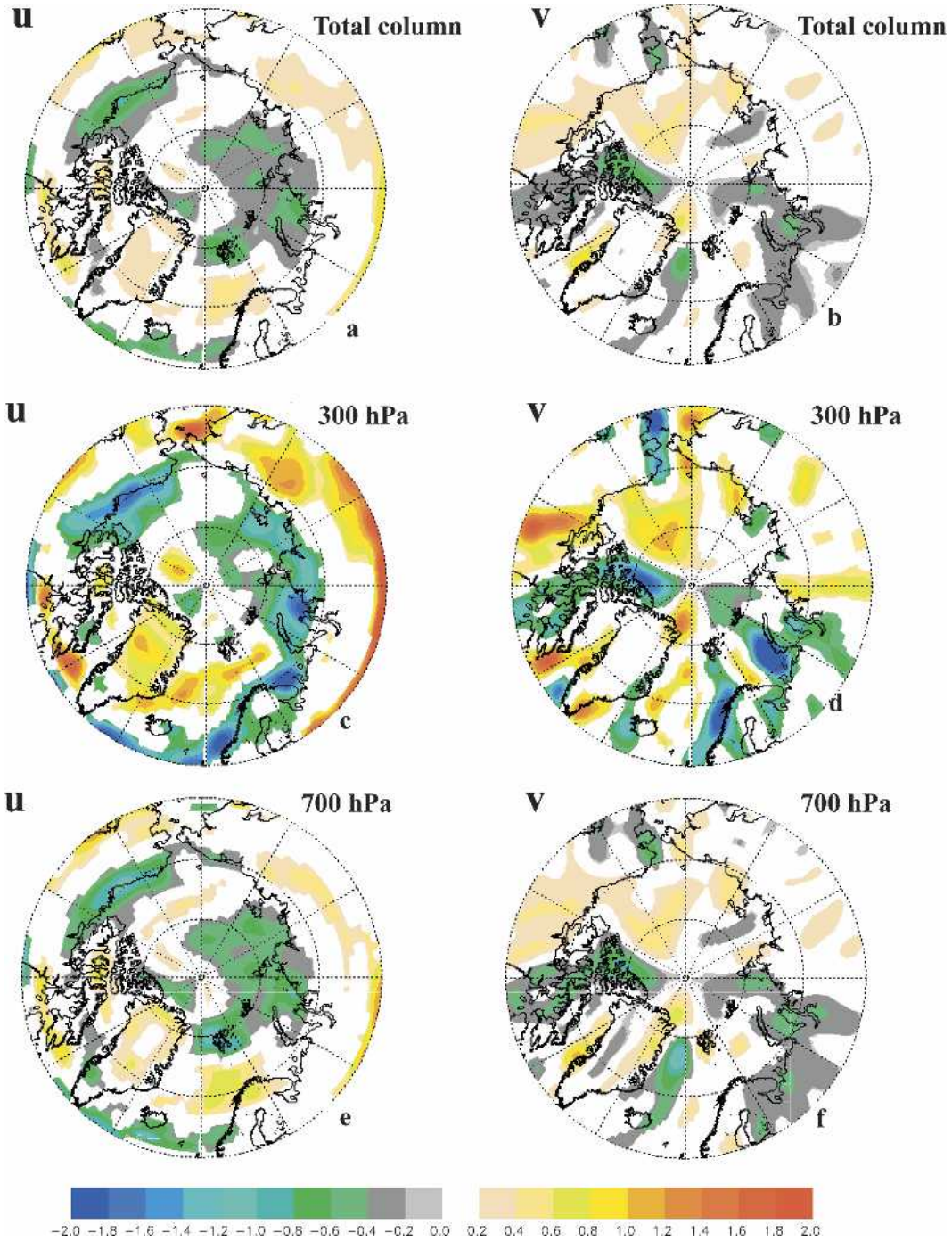

FIG. 6. The 22.5-yr trends (mid-1979–2001) in (left) zonal and (right) meridional wind derived from TOVS temperature profiles over the entire year. (top) The total troposphere (surface to 300 hPa), (middle) the 300-hPa level, and (bottom) the 700-hPa level. Units are m s^{-1} $decade^{-1}$. Only trend values with confidence larger than 90% are plotted.

that at 700 hPa because the mass-weighted center of the 1000–300-hPa column is at 650 hPa. In the lower troposphere (represented by the plot for 700 hPa), the trend patterns are consistent with the shift in the Beaufort gyre from the 1980s to the 1990s identified by Rigor et al. (2002) using satellite-monitored motions of buoys on the pack ice during winter. They found that during the 1990s the transport shifted eastward in the Barents–

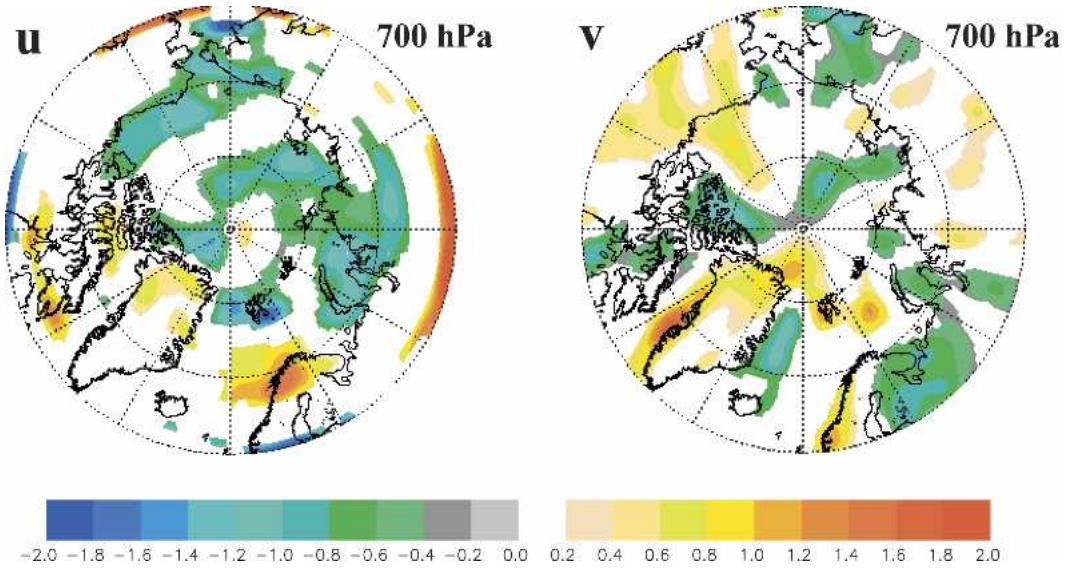

FIG. 7. Winter [Dec–Feb (DJF)] decadal trends during 1979–2001 for (left) zonal and (right) meridional winds at 700 hPa calculated from TOVS-retrieved temperature profiles. Units are m s^{-1} $decade^{-1}$. Trends with confidence exceeding 90% are plotted.

Kara Seas, increased northward in the Siberian Sea, and was stronger southward through the Fram Strait as compared to the previous decade.

Figures 7–10 present trends in u and v calculated for each season at the 700-hPa level. Upper-level winds are not shown, as patterns in the trends at 300 hPa are well correlated spatially with those at 700 hPa (see seasonal correlation coefficients in Table 2), further evidence that the Arctic (the region north of 60°N) tends to be barotropic. A comparison of the patterns among the seasons, however, reveals some persistent characteristics as well as some seasonally varying features.

The zonal component (u) exhibits a moderate degree of similarity through the seasons. Spatial correlation coefficients between seasonal trends are computed by correlating trend values at each grid point in the domain north of 60°N for the two fields and are presented in Tables 3 and 4 for the 700- and 300-hPa levels. The

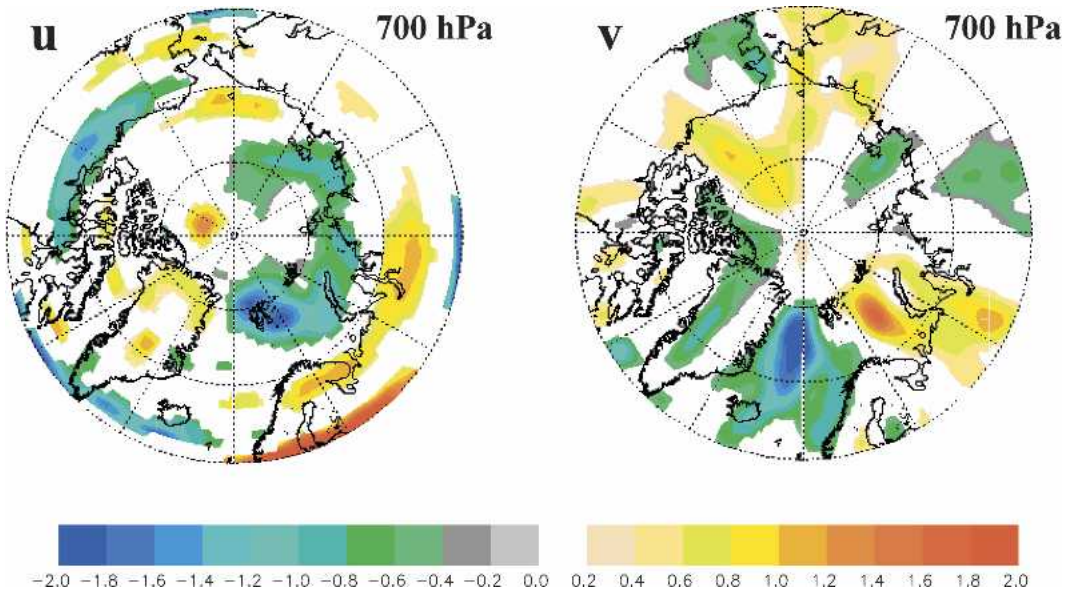

FIG. 8. Same as in Fig. 7 but for spring [Mar–May (MAM)].

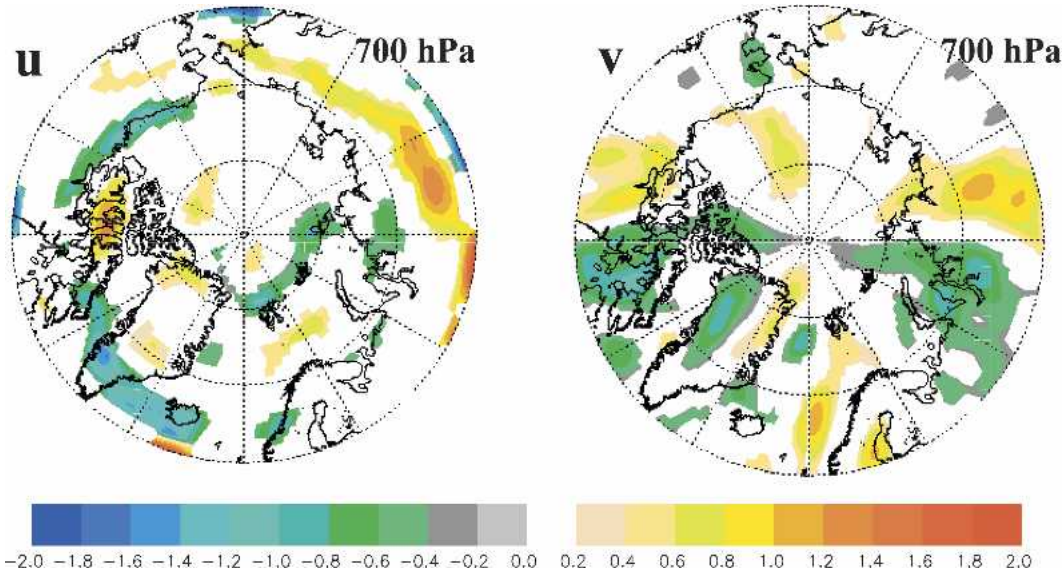

FIG. 9. Same as in Fig. 7 but for summer [Jun–Aug (JJA)].

summer season exhibits only small trend values. The eastern Arctic Ocean is characterized by decreasing westerly winds through most of the year, while winds are more westerly in the Greenland Sea area during autumn and winter. An area with consistent negative trends appears along the coasts of northwest Canada and northern Alaska. Confidence in this feature is weaker, however, as orographic effects likely play a role in low-level winds, and trends in winds from the NCEP–NCAR reanalysis show less consistency with TOVS-derived patterns. In general, the Arctic Ocean is dominated by negative trends in autumn and winter, indicating a weakening or perhaps shifting of the polar vortex.

Trend patterns in the meridional component (v) are shown on the right-hand side in Figs. 7–10. Spring stands out as having a different pattern from the other seasons (consistent with low correlation coefficients in Tables 3 and 4), with a strong increase in southerly winds on the Pacific side of the Arctic, which is consistent with the distinct spring warming trend in the lower troposphere diagnosed by Overland et al. (2002) from

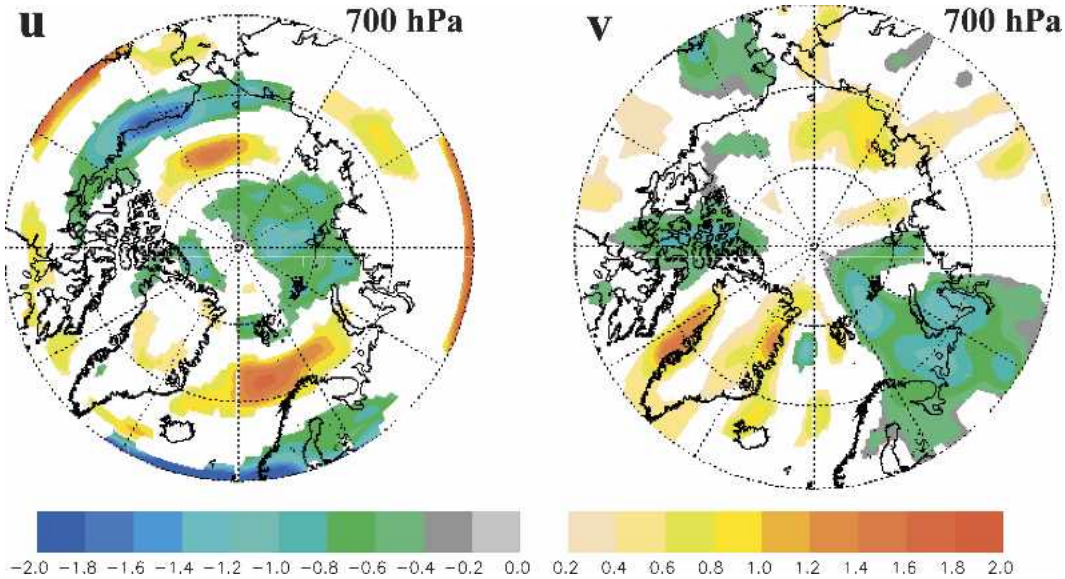

FIG. 10. Same as in Fig. 7 but for autumn [Sep–Nov (SON)].

TABLE 2. Spatial correlation coefficients between trends in winds at 300 and 700 hPa. Three-month ranges are signified by the first letter of each respective month.

Wind component	DJF	MAM	JJA	SON	Annual
Zonal (u)	0.76	0.79	0.62	0.83	0.68
Meridional (v)	0.69	0.78	0.57	0.81	0.57

TOVS Path-P retrievals and NCEP–NCAR reanalyses. Spring is also characterized by strong positive trends in the Barents–Kara Seas as well as negative trends over the Greenland–Iceland–Norway (GIN) Seas. Correlations between spring trends and values for other seasons as well as the annual trend are consistently weak for both u and v components, suggesting that changes in the spring circulation may result from forcings or interactions that are different from the rest of the year. One candidate is a change in surface melt onset, which corresponds to a sharp decrease in surface albedo and surface-absorbed solar radiation. The stratification of the atmospheric boundary layer consequently decreases as the surface warms to the melting point and surface temperature is less tightly coupled to the downwelling longwave radiation, which allows more mixing of upper-level winds down to the surface. Satellite-derived estimates of melt-onset date by Belchansky et al. (2004) indicate that melting occurred 10–20 days earlier during the 1990s versus the 1980s in the Pacific sector of the Arctic where TOVS-derived meridional winds exhibit significant positive trends in spring (Fig. 8). Negative trends in v winds over the Laptev Sea in winter and spring coincide with later melt-onset dates in their analysis. A definite causal relationship cannot be implicated at this time, but the correspondence is suggestive of a process responsible for the distinctive patterns in spring trends.

The summer–autumn patterns in the v component display several common features, as well, particularly in the Barents–Kara sector, where a large area of negative trend (more northerly wind) appears. Southerly trends in the Siberian Sea in spring and autumn implicate a possible mechanism for dynamic sea ice removal in an area where decreasing sea ice concentrations have been observed (e.g., Comiso 2002; Parkinson and Cavalieri 2002). In spring the Barents Sea exhibits positive trends, coinciding with the breakup of annual ice, and consequently this area may be more susceptible to dynamic ice removal than in other seasons. Meridional atmospheric temperature gradients are large in late spring as the land warms before the ocean, thus positive trends in v likely translate to stronger poleward heat advection. Northerly trends in the Lincoln Sea (north of the Canadian Archipelago) may contribute to observed increases in ice concentrations in this area, while the northerly trends in the western GIN Seas, especially in spring, likely contribute to increased ice advection and observed concentration decreases in this area.

TABLE 3. Spatial correlations between seasonal and annual trends at 700 hPa. The values below the diagonal of blanks in the lower left of the table are for u and those in the upper right are for v. For example, the first value in the DJF column is the correlation between the trend in the u component in winter and spring, while the first value in the DJF row is the correlation between the trend in the v component in winter and spring.

	DJF	MAM	JJA	SON	Annual
DJF	—	0.14	0.34	0.31	0.71
MAM	0.10	—	0.15	−0.14	0.46
JJA	0.15	0.28	—	0.43	0.73
SON	0.46	0.03	0.20	—	0.64
Annual	0.70	0.54	0.57	0.71	—

TABLE 4. Same as in Table 3 but for the 300-hPa level.

	DJF	MAM	JJA	SON	Annual
DJF	—	−0.05	0.37	0.38	0.68
MAM	0.04	—	0.07	−0.21	0.33
JJA	0.34	0.19	—	0.46	0.78
SON	0.48	0.03	0.38	—	0.67
Annual	0.71	0.46	0.71	0.75	—

c. *Time series and anomalies*

While the trends are intriguing and appear to be related to observed changes in other variables over the past two decades, there is also a large amount of interannual variability punctuated with strong anomalies. Six representative regions of the Arctic Ocean, defined in Table 1 and illustrated in Fig. 1, are selected to investigate temporal behavior of the winds. The regions are chosen because they exhibit significant and differing trends.

Monthly anomalies are calculated by subtracting the 22.5-yr mean for each month from the mean for each individual month. Figures 11 and 12 display time–height anomalies of u and v component winds for the six regions. The meridional component is not shown for the North Pole region, as any flow will result in positive and negative values cancelling each other. Overall, it is clear from the patterns of anomalies in Figs. 11 and 12 that the trends displayed in Fig. 6 are due to a temporal behavior that is far from monotonic; rather they result from episodic periods of fluctuating anomalies. Values increase in strength with height, corresponding to the increase in wind speed with height.

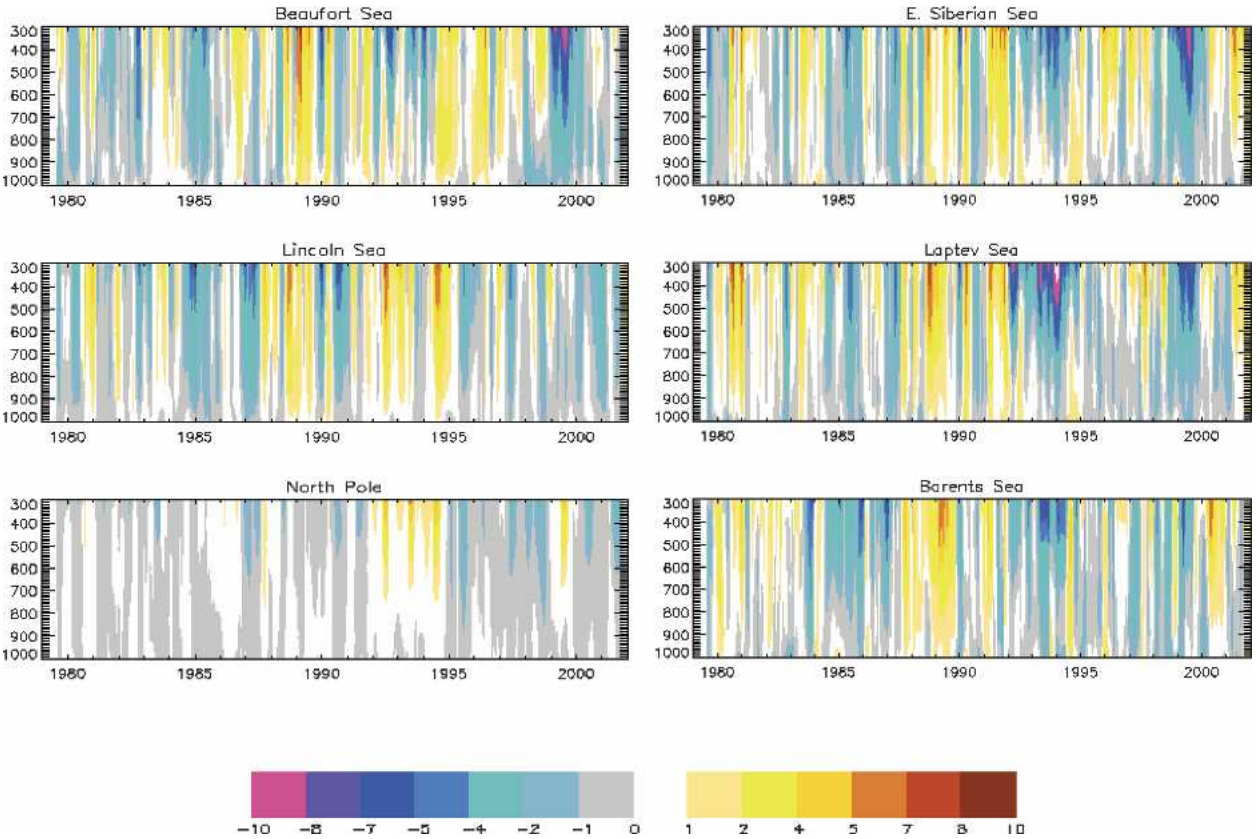

FIG. 11. Zonal wind anomalies from 1979 to 2001 in regions defined in Fig. 1.

Zonal winds in the eastern Arctic (right-hand side in Fig. 11) exhibit a fairly distinct decadal-scale cycle. Positive (westerly) anomalies are prevalent from approximately 1980–84, mid-1987–92, mid-1994–97, and from 2000 onward. Negative anomalies are evident between these periods, particularly in the mid-1990s. The pattern is best defined in the Barents and Laptev Seas, suggesting it is related to a shift in the Icelandic low pressure center. In the western Arctic, the decadal signal in zonal wind is somewhat less pronounced, but the strong positive anomalies seen in the east during the late 1980s are evident, particularly in the Beaufort and Lincoln Seas. Strong negative wind anomalies on both sides of the date line occur during 1999, where they correspond to a large negative anomaly in 300-hPa heights over the Chukchi Sea as depicted in the NCEP–NCAR reanalysis (not shown). Positive anomalies in u occur in the North Pole region during the mid-1990s in association with a negative height anomaly on the date line at about 75°N and the associated enhanced cyclonic flow. This pattern is also responsible for the conspicuous negative u anomalies in the eastern Arctic regions.

In general the meridional anomalies (Fig. 12) are less cohesive than the zonal values, with the notable exception of the Lincoln Sea. In this area the anomalies are positive for the earlier half of the data record, after which strong negative values occur in the mid-1990s from 1993 to 1996 and during 1999. These features account for the negative trend in the Lincoln Sea area exhibited in Fig. 6d. In the Beaufort and east Siberian Seas the tendency is opposite, that is, there is an overall switch from predominantly negative anomalies to more frequent positive values, contributing to positive trends in these regions. These observations may help explain the strong signal of decreasing ice extent in the east Siberian Sea and increasing ice extent north of the Canadian Archipelago.

One might suspect that these observed anomalies are related to the North Atlantic Oscillation (NAO; e.g., Hurrell et al. 2003). The winter (January–March) NAO index for 1980–2001 (from Osborn et al. 1999) is correlated with winter anomalies of u and v wind components at 700 hPa (Table 5). In the Barents Sea region, where the strongest NAO influence might be expected, correlations with the zonal wind are moderate but significant (maximum of -0.36 at a lag of -1 yr, i.e., the NAO index lags behind the anomaly), while correlations with the meridional wind are stronger: 0.48 at zero

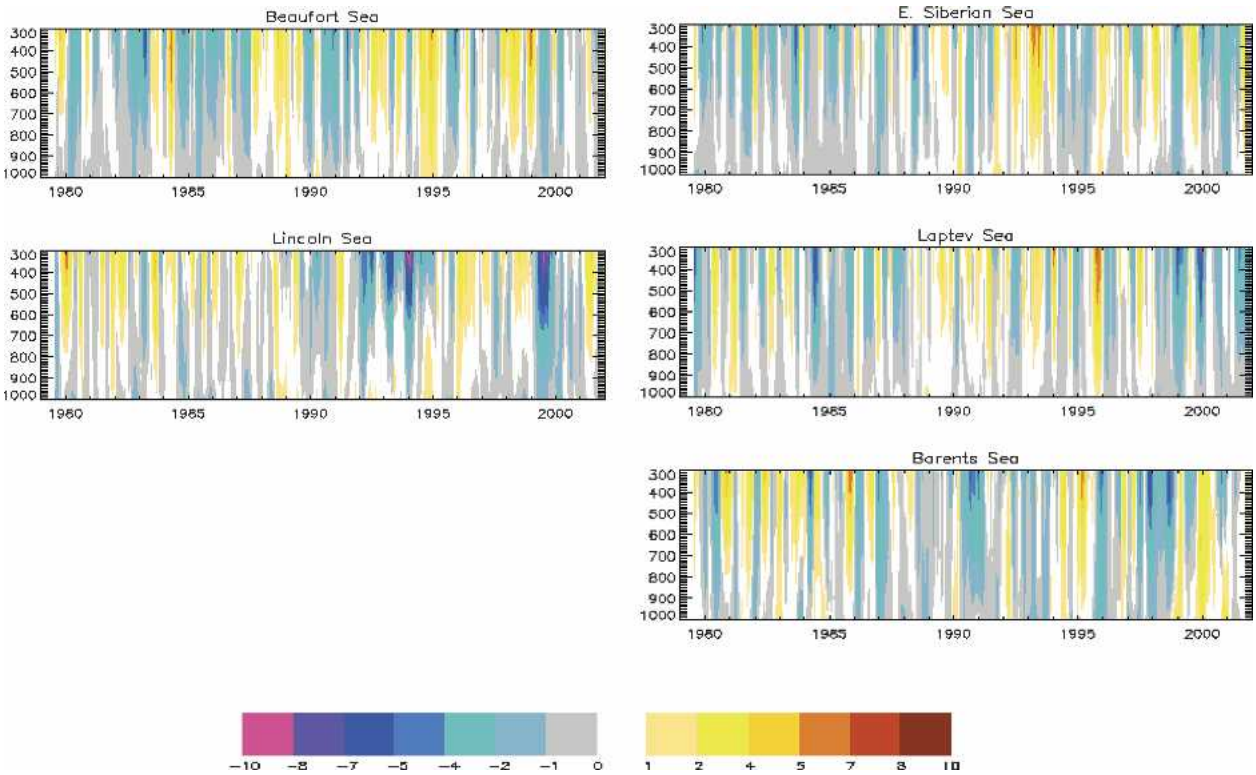

FIG. 12. Meridional wind anomalies from 1979 to 2001 in regions defined in Fig. 1.

lag. Farther downstream in the Laptev and east Siberian Seas, the NAO index leads zonal wind anomalies with moderate but significant positive correlations. In the Lincoln Sea correlations with the *u* component are again significant but moderate (0.43 and 0.41 at lags of −1 and 0), while the meridional winds exhibit a correlation of −0.59 at zero lag. These results suggest that the NAO has a moderate relationship with wind changes in the Atlantic sector of the Arctic. A continued positive NAO regime may signal further sea ice decreases in the Barents Sea caused by stronger southerly winds, accompanied by further increases in concentration north of the Canadian Archipelago and Greenland owing to increased northerly and westerly (both onshore) winds. As discussed previously, however, winds in the spring season appear to correspond more closely with changes in sea ice extent than do winter winds.

TABLE 5. Lagged rank (Spearman's) correlations between the winter NAO index and mean winter anomalies of *u* and *v* winds at 700 hPa. A lag = 1 denotes that the NAO index leads the wind anomaly by 1 yr. Regions are defined in Fig. 1. Significant values (>90% confidence according to an *f* test) are indicated with bold type.

	u			*v*		
Region	−1	0	1	−1	0	1
Barents Sea	**−0.36**	−0.27	−0.17	−0.22	**0.48**	−0.01
Laptev Sea	0.00	0.18	**−0.59**	0.06	0.18	−0.35
East Siberian Sea	−0.02	0.04	**−0.46**	0.32	0.24	−0.04
Beaufort Sea	0.06	0.08	−0.20	0.09	0.24	−0.17
Lincoln Sea	**0.43**	**0.41**	−0.30	−0.12	**−0.59**	−0.16
North Pole	**0.45**	−0.23	0.07	−0.23	0.01	**−0.37**

4. Conclusions

Recent studies have revealed significant changes in the Arctic circulation in the past few decades, but also that upper-level winds over the Arctic Ocean from operational reanalyses exhibit large biases relative to rawinsonde measurements. Reliable wind fields are essential for accurate calculations of atmospheric transport of heat, moisture, and pollutants, as well as for understanding relationships among changing atmospheric and surface parameters. In an attempt to improve upon this situation, a new 22.5-yr (mid-1979–2001) product of three-dimensional wind fields in the Arctic troposphere has been generated from satellite-derived temperature soundings. The daily-mean fields, centered on 1200

UTC, are produced on a $1° \times 1°$ latitude–longitude grid for the region north of 60°N. Ten-meter winds from the NCEP–NCAR reanalysis are used for the lower boundary, and first-guess thermal-wind profiles calculated from the temperature retrievals are corrected with a mass-conservation technique developed by ZVW2.

Validation against rawinsondes from the yearlong Surface Heat Budget of the Arctic (SHEBA) field campaign in the Beaufort Sea reveals that wind speed–normalized biases are near zero in the poleward component, as compared to biases of over 50% for winds from the NCEP–NCAR and ECMWF reanalysis products. This is very encouraging for applications to poleward advection calculations. Biases in the zonal component are also smaller than those for reanalyses above 600 hPa. Remaining differences from rawinsondes, particularly the zonal wind below 600 hPa, are attributed to uncertainties in rawinsonde wind measurements (2–3 $m\ s^{-1}$), errors in satellite-retrieved temperature profiles, and barrier effects of Greenland in the zonal wind flow, which enter into the mass-conservation calculation. Future efforts will explore using upper-level wind velocities retrieved from satellite-observed features (e.g., Key et al. 2003), which could provide an upper tie point in the wind profile.

Trends and anomalies for the 22.5-yr record are calculated from the satellite-derived wind fields. Annual-mean trends in both u and v components at varying levels are well correlated, suggesting that the Arctic atmosphere is nearly barotropic. On annual average the zonal winds exhibit positive trends (more westerly) over most of Eurasia between 60° and 70°N, while winds are weaker from the west over the eastern Arctic Ocean and northwestern Canada/Alaska. A corresponding pattern appears in the meridional trends, which suggests that the polar vortex has shifted toward northern Canada. Increased offshore winds in the east Siberian Sea, as well as in the Barents Sea during spring and summer, may aid in explaining observed decreases in sea ice extent in those areas.

A separation of trends into the four seasons reveals that many features persist through the year, while some vary in strength and sign. Positive zonal trends appear over Eurasia and negative values over the eastern Arctic Ocean in all seasons. The patterns in both u and v trends during spring are distinctive from those in other seasons, as quantified by low correlation coefficients. Spring patterns in meridional trends appear to correspond with observed changes in melt-onset date, which may implicate a spring-only interaction responsible for the seasonal differentiation in trends. Dynamic forcing of sea ice may be stronger in spring, when first-year ice is breaking up and the boundary layer stratification is weakening, implying that trends in spring winds may have a stronger relationship with observed changes in sea ice concentration. Indeed the spring v-component trends appear to agree well with sea ice change: increased southerly flow at 700 hPa corresponds with decreased ice concentrations in the east Siberian and Barents Seas, while increased northerly flow occurs where ice has increased north of the Canadian Archipelago and where decreased ice cover is observed in the western GIN Seas. Increased advective heating may also play a role where stronger southerly flow interacts with steep horizontal temperature gradients in spring.

Anomalies in the zonal wind profiles exhibit a decadal-scale cycle in the eastern Arctic Ocean and less so in the west. Strong anomalies in u and v punctuate the record, and contribute significantly to observed trends. Because the data record is relatively short, a year with a strong anomaly can have a significant effect on the trend. Anomalies in the meridional component appear to have shifted from primarily positive to negative in the Lincoln Sea, while the opposite tendency is observed in the east Siberian and Beaufort Seas. These tendencies manifest themselves in the trend patterns.

Anomalies in the winter meridional winds in the Atlantic sector of the Arctic show moderate correlation with the winter NAO index. Anomalies in the eastern (western) Arctic are positively (negatively) correlated with the index, suggesting that a continuation of the positive NAO regime may lead to further decreases in sea ice in the Barents–Kara Seas and increases along the Canadian Archipelago. Trends in TOVS-derived winds suggest, however, that a stronger relationship may exist between spring patterns and sea ice extent changes.

In summary, a new three-dimensional wind product has been generated from 22.5 yr of satellite temperature retrievals over the Arctic Ocean. Accuracies appear to surpass winds from reanalyses, particularly in the poleward direction, which will increase confidence in studies of Arctic atmospheric circulation features. In particular, improved wind fields will increase the accuracy of calculated heat and moisture transport into and within the Arctic from lower latitudes, which constitutes the single largest source of energy for the Arctic climate system.

Acknowledgments. The authors are very grateful to the anonymous reviewer and to the editor, Dr. Siegfried Schubert, for their valuable and constructive suggestions. This work was supported by Grants OPP-0105461 and OPP-0240791 from NSF and UAF02-0032 from NOAA/University of Alaska. The contents of this paper are solely the opinions of the authors and do not

constitute a statement of policy, decision, or position on behalf of NOAA or the U.S. government.

REFERENCES

Atlas, R., R. N. Hoffman, S. C. Bloom, J. C. Jusem, and J. Ardizzone, 1996: A multiyear global surface wind velocity data set using SSM/I wind observations. *Bull. Amer. Meteor. Soc.,* **77,** 869–882.

Belchansky, G. I., D. C. Douglas, and N. G. Platonov, 2004: Duration of the Arctic sea ice melt season: Regional and interannual variability, 1979–2001. *J. Climate,* **17,** 67–80.

Carle, W. E., and J. R. Scoggins, 1981: Determination of wind from *Nimbus-6* satellite sounding data. NASA Reference Publication 1072, 72 pp.

CEAREX Drift Group, 1990: CEAREX Drift Experiment. *Eos, Trans. Amer. Geophys. Union,* **71,** 1115–1118.

Chédin, A., N. A. Scott, C. Wahiche, and P. Moulinier, 1985: The improved initialization inversion method: A high resolution physical method for temperature retrievals from satellites of the TIROS-N series. *J. Climate Appl. Meteor.,* **24,** 128–143.

Comiso, J. C., 2002: A rapidly declining perennial sea ice cover in the Arctic. *Geophys. Res. Lett.,* **29,** 1956, doi:10.1029/2002GL015650.

Francis, J. A., 1994: Improvements to TOVS retrievals over sea ice and applications to estimating Arctic energy fluxes. *J. Geophys. Res.,* **99,** 10 395–10 408.

——, 2002: Validation of reanalysis upper-level winds in the Arctic with independent rawinsonde data. *Geophys. Res. Lett.,* **29,** 1315, doi:10.1029/2001GL014578.

——, and A. J. Schweiger, cited 1999: TOVS Pathfinder Path-P daily Arctic gridded atmospheric parameters. National Snow and Ice Data Center. [Available online at http://nsidc.org/data/nsidc-0027.html.]

——, and A. J. Schweiger, 2000: A new window opens on the Arctic. *Eos, Trans. Amer. Geophys. Union,* **81,** 77–78.

Hurrell, J. W., Y. Kushnir, G. Ottersen, and M. Visbeck, 2003: An overview of the North Atlantic Oscillation. *The North Atlantic Oscillation: Climate Significance and Environmental Impact, Geophys. Monogr.,* Vol. 134, Amer. Geophys. Union, 1–35.

Key, J. R., D. Santek, C. S. Velden, N. Bormann, J.-N. Thepaut, L. P. Riishojgaard, Y. Zhu, and W. P. Menzel, 2003: Cloud-drift and water vapor winds in the polar regions from MODIS. *IEEE Trans. Geosci. Remote Sens.,* **41,** 482–492.

Kistler, R., and Coauthors, 2001: The NCEP/NCAR 50-year reanalysis: Monthly means CD-ROM and documentation. *Bull. Amer. Meteor. Soc.,* **82,** 247–267.

LeadEx Group, 1993: The Lead Experiment. *Eos, Trans. Amer. Geophys. Union,* **74,** 393–397.

Moyer, V., J. R. Scoggins, N.-M. Chou, and G. S. Wilson, 1978: Atmospheric structure deduced from routine *Nimbus-6* satellite data. *Mon. Wea. Rev.,* **106,** 1340–1352.

Osborn, T. J., K. R. Briffa, S. F. B. Tett, P. D. Jones, and R. M. Trigo, 1999: Evaluation of the North Atlantic Oscillation as simulated by a coupled climate model. *Climate Dyn.,* **15,** 685–702.

Overland, J. E., M. Wang, and N. A. Bond, 2002: Recent temperature changes in the western Arctic during spring. *J. Climate,* **15,** 1702–1716.

——, M. C. Spillane, and N. N. Soreide, 2003: Integrated analysis of physical and biological pan-Arctic change. *Climate Change,* **63,** 291–322.

Overpeck, J. T., and Coauthors, 1997: Arctic environmental change of the last four centuries. *Science,* **278,** 1251–1256.

Parkinson, C. L., and D. J. Cavalieri, 2002: A 21 year record of arctic sea-ice extents and their regional, seasonal and monthly variability and trends. *Ann. Glaciol.,* **34,** 441–446.

Peterson, R. A., and L. H. Horn, 1977: An evaluation of 500 mb height and geostrophic wind fields derived from *Nimbus-6* soundings. *Bull. Amer. Meteor. Soc.,* **58,** 1195–1201.

Rigor, I. G., R. L. Colony, and S. Martin, 2000: Variations in surface air temperature in the Arctic, 1979–97. *J. Climate,* **13,** 896–914.

——, J. M. Wallace, and R. L. Colony, 2002: Response of sea ice to the Arctic Oscillation. *J. Climate,* **15,** 2648–2663.

Schweiger, A. J., R. W. Lindsay, J. A. Francis, J. Key, J. Intrieri, and M. Shupe, 2002: Validation of TOVS Path-P data during SHEBA. *J. Geophys. Res.,* **107,** 8041, doi:10.1029/2000JC000453.

Scott, N. A., and Coauthors, 1999: Characteristics of the TOVS Pathfinder Path-B dataset. *Bull. Amer. Meteor. Soc.,* **80,** 2679–2701.

Serreze, M., cited 1997: Comprehensive ocean-atmosphere data set LMRF arctic subset. National Snow and Ice Data Center. [Available online at http://nsidc.org/data/nsidc-0057.html.]

——, and Coauthors, 2000: Observational evidence of recent change in the northern high-latitude environment. *Climate Change,* **46,** 159–207.

Slonaker, R. L., and M. L. Van Woert, 1999: Atmospheric moisture transport across the Southern Ocean via satellite observations. *J. Geophys. Res.,* **104,** 9229–9249.

Susskind, J., P. Piriano, L. Rokke, L. Iredell, and A. Mehta, 1997: Characteristics of the TOVS Path A dataset. *Bull. Amer. Meteor. Soc.,* **78,** 1449–1472.

Uttal, T., and Coauthors, 2002: The Surface Heat Budget of the Arctic Ocean. *Bull. Amer. Meteor. Soc.,* **83,** 255–276.

Wallace, J. M., and P. V. Hobbs, 1977: *Atmospheric Science: An Introductory Survey.* Academic Press, 467 pp.

Walsh, J. E., W. L. Chapman, and T. L. Shy, 1996: Recent decrease of sea level pressure in the central Arctic. *J. Climate,* **9,** 480–486.

Wang, S.-H., J. A. Francis, and D. H. Bromwich, 2003: Evaluation of the NCEP/NCAR and ECMWF 15-year reanalyses over the data-sparse Arctic Ocean. Preprints, *Seventh Conf. on Polar Meteorology and Oceanography*, Hyannis, MA, Amer. Meteor. Soc., CD-ROM, P1.7.

Zou, C.-Z., and M. L. Van Woert, 2001: The role of conservation of mass in the satellite-derived poleward moisture transport over the Southern Ocean. *J. Climate,* **14,** 997–1016.

——, and ——, 2002: Atmospheric wind retrievals from satellite soundings over the middle- and high-latitude oceans. *Mon. Wea. Rev.,* **130,** 1771–1791.